

ChemComm

Accepted Manuscript



This is an *Accepted Manuscript*, which has been through the Royal Society of Chemistry peer review process and has been accepted for publication.

Accepted Manuscripts are published online shortly after acceptance, before technical editing, formatting and proof reading. Using this free service, authors can make their results available to the community, in citable form, before we publish the edited article. We will replace this *Accepted Manuscript* with the edited and formatted *Advance Article* as soon as it is available.

You can find more information about *Accepted Manuscripts* in the [Information for Authors](#).

Please note that technical editing may introduce minor changes to the text and/or graphics, which may alter content. The journal's standard [Terms & Conditions](#) and the [Ethical guidelines](#) still apply. In no event shall the Royal Society of Chemistry be held responsible for any errors or omissions in this *Accepted Manuscript* or any consequences arising from the use of any information it contains.

COMMUNICATION

Photo-thermal plasmonic effect in spin crossover@silica/gold nanocomposites

Cite this: DOI: 10.1039/x0xx00000x

Iurii Suleimanov,^{a,b} José Sánchez Costa,^a Gábor Molnár,^a Lionel Salmon,^{a*} and Azzedine Bousseksou^{a*}

Received 00th January 2012,

Accepted 00th January 2012

DOI: 10.1039/x0xx00000x

www.rsc.org/

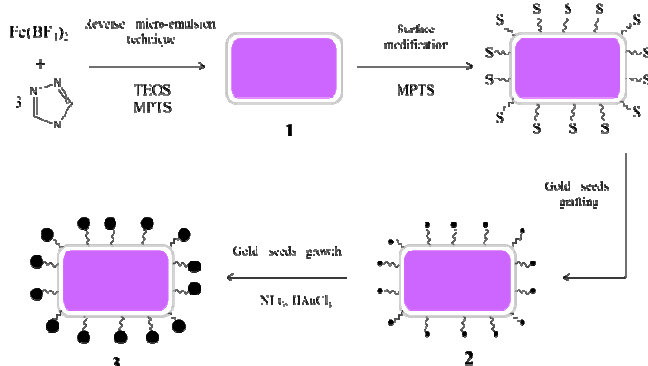
Nanocomposite spin crossover (SCO) materials with gold nanoparticles (Nps) - displaying both electronic bistability and plasmonic properties - were synthesized and a plasmon-enhanced photothermal spin state switching was evidenced. Using this effect, we demonstrated a three times reduction of the laser power needed for switching the new SCO@SiO₂/gold nanocomposite compared to the pure coordination polymers.

Nanocomposite materials include two or more moieties from which at least one has dimensions in the nanometer (1-100) size regime. Commonly one of these compounds is inorganic and the other one organic in nature.¹ By controlling their mutual arrangement, the most noticeable advantage of inorganic-organic nanocomposites is that they can satisfactorily combine properties of organic and inorganic components in one material² with the additional possibility to present synergetic effects and thus properties which are unknown in the parent constituent materials. Following this strategy new nanocomposite materials were developed from a switchable molecular-based material with the objective to diminish the laser power needed for a complete spin state switching process. Indeed, such reduction of the threshold laser power could overcome one of the major technological limitations encountered for SCO compounds.³ SCO compounds⁴ are a class of functional materials containing a transition metal ion, able to reversibly switch their spin state upon external stimuli such as variations of temperature and/or pressure, magnetic field and light irradiation amongst others.⁵ The reversible switch between the high- and low-spin states can be interpreted as a binary code, making of the SCO compounds ideal candidates for nanoelectronics and nanophotonics at reduced scales, down to the single molecule level.⁶ This exciting and burgeoning field has led very recently to the increase of the number of publications reporting the elaboration of such materials organized in thin films or nanoparticles.⁷ In this context we employed recently the plasmonic effect with the aim of detecting the spin state switching at the nanometer scale through the refractive index change associated with the spin crossover.^{8,9} In addition, a synergy between the two phenomena was also observed⁹ and attempts for plasmonic enhancement of the Raman signal of SCO molecules were also reported.¹⁰⁻¹²

In the present study, we associated SCO materials with gold nanoparticles by means of an intermediate decorated silica shell. The SCO nanocomposite particles are combined with gold with the aim of using the ability of gold nanoparticles to absorb light and convert it to heat. This plasmonic heating effect is a fascinating property and has been employed in different fields of material science¹³ and biomedicine.¹⁴

The nanocomposite core-shell SCO particles are synthesized from the coordination polymer [Fe(trz)(H-trz)₂](BF₄) (H-trz = 1,2,4-triazole and trz = 1,2,4-triazolato), known to show a memory effect above room temperature¹⁵ using silica for grafting the gold NPs. A schematic overview of the formation of the nanocomposite particles described in this communication is shown in Scheme 1. The use of silica is of great interest because of their high porosity and the possibility of grafting on the surface others functionalities. In addition, silica does not interfere with the SCO properties.^{16,17,18} The preparation of the silica-SCO NPs was achieved following a recent strategy introduced by Padilla and co-authors (see detailed synthesis in the SI).¹⁸ Briefly, SCO@SiO₂ particles were synthesized by the reverse-micelle technique mixing two micro-emulsions using Triton and TEOS (tetraethylorthosilicate) as tensioactive and silica source respectively, and integrating in one hand the triazole ligand and in the other hand the iron(II) salt. In comparison with the published result,¹⁸ we have voluntarily reduced the quantity of the silica precursor in order to reach a whole coverage but a thinner layer of the shell and thus favor the plasmonic heating effect. After mixing and stirring for 24h the obtained microemulsion, multiple washing steps were employed to obtain surfactant-free SCO@SiO₂ NPs, hereby named sample **1** (fig. 1a). The next step consisted to associate these composite particles with small gold particles. Examples of modification of silica particles with gold nanoparticles and subsequent shell growth have been already reported.¹⁹ In our case, the surface functionalization process of **1** was achieved using MPTS (MPTS = 3-mercaptopropyl-trimethoxysilane). It is interesting to note that the surface regularity of the NPs has been also improved by adding MPTS during the reverse-micelle process (see in fig. S2 the influence of the incorporation of MPTS during the micellar exchange). The nature of the SiO₂ shell was confirmed by FT-IR spectroscopy, showing spectral bands characteristic for SiO₂ (see fig. S1). The gold functionalization of the SCO@SiO₂ particles was achieved using fresh preformed 2 nm gold NPs (see TEM images in

fig. S3) obtained by the classical Duft method,²⁰ leading to sample **2** (fig. 1b). Aiming to increase the size of the gold seeds attached to the surface on **2**, additional reduction of aurum salt was performed using triethylamine in a non-aqueous media to avoid the oxidation of the SCO moieties. As a result, increasing gold particle size was observed in the corresponding sample **3** (fig. 1c).



Scheme 1. Synthesis steps of the nanocomposites

The obtained particles were isolated and their morphology and properties were fully characterized using physico-chemical methods. Transmission electron microscopy (TEM) images for sample **1** reveal fairly monodisperse rod-like nanoparticles with an average width of 88 ± 18 and length 154 ± 10 nm (fig. 1a and fig. S2). The electron microscopy contrast between the silica and the SCO materials permits us to conclude that this latter is well embedded in a silica shell. This result is clearly confirmed by the high resolution scanning transmission electron microscopy coupled quantified energy dispersive X-ray spectroscopy (HR STEM EDX) analyses (fig. S4). Similar TEM measurements on sample **2** (fig. 1b and fig. S5) and **3** (fig. 1c and fig. S6), reveal the presence of small gold seeds attached to SCO@SiO₂ particles and their growth when passing from sample **2** to sample **3**. (An increase of the mean diameter of the gold nanoparticles from 2 to 14 nm is observed.) Moreover, we can observe the maintaining of the SCO@SiO₂ particle shape and size during the grafting and the growth of gold nanoparticles. Figure 1d presents the STEM EDX mapping of a nanocomposite particle of **3**, which undoubtedly confirms the core/shell architecture of the particles and the grafting of the gold nanoparticles.

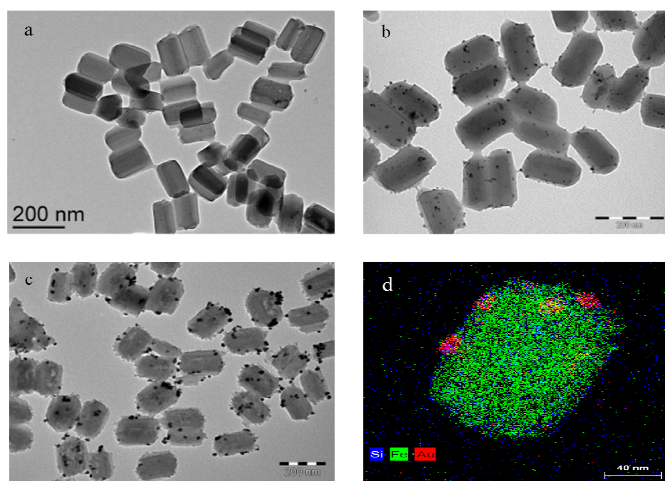


Figure 1. TEM images for **1** (a), **2** (b) and **3** (c) and (d) STEM-EDX mapping of a nanoparticle from sample **3**, the colour code is: iron

(green), silicon (blue) and red (gold).

See also figures S7 - S10 for complementary HRTEM, EDX and darkfield STEM images as well as STEM EDX compositional maps for samples **2** and **3**.

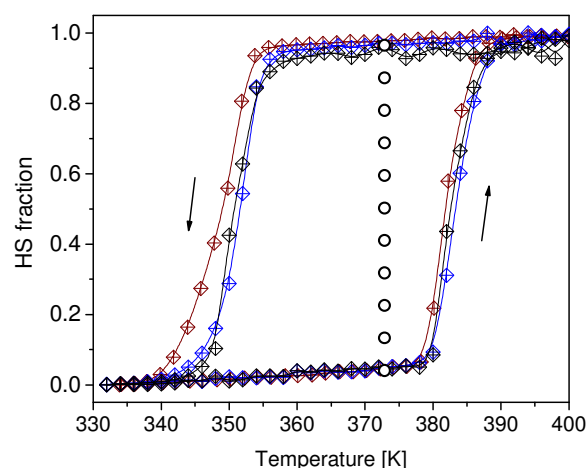


Figure 2. Temperature dependence of the HS fraction for samples **1**, **2** and **3** (red, black and blue colours, respectively) on heating and cooling (second thermal cycle)

Magnetic susceptibility of **1-3** was measured by means of a SQUID magnetometer on cooling and heating in the 300 to 400 K temperature range under a magnetic field of 0.1 T. (See fig. S11 and fig. S12 for several consecutive thermal cycles using both magnetometry and optical reflectivity to detect the spin transition.) The hysteretic behaviour of the spin transition of the SCO coordination polymer is maintained with almost the same hysteresis loop width (45 K) for the three samples, which is slightly smaller compared to the bulk analogue (50 K)²¹. The second thermal cycle leads systematically to a smaller hysteresis width (35 K), which becomes stable for further cycling. This “run-in effect” is typical for many SCO compounds and was already reported for [Fe(trz)(H-trz)₂](BF₄)₂.²² This phenomenon may be related to the loss of residual (post-synthetic) solvent molecules. Figure 2 illustrates the corresponding HS fraction (n_{HS}) as a function of T for the second (stable) thermal cycle for the three samples. These curves were obtained by neglecting any LS and HS residual fractions at high and low temperatures, respectively. This assumption is clearly supported by the Mössbauer (fig. S13) and Raman (fig. S14 – S17) spectra of the samples.

A series of Raman experiments were performed on samples **1-3** aiming to investigate the plasmonic heating process. All the samples were implemented in a similar manner (the powder sample were compacted to obtain a dense and homogeneous thin layer), in order to try to keep similar the heat transfer conditions. To investigate the laser-induced spin state switching and the plasmonic heating effect a series of Raman spectra were taken for sample **1** (SCO@silica) and **2** (SCO@silica/small gold Nps) initially kept at 373 K in the LS state (temperature chosen in the hysteresis loop, see fig. 2) and varying progressively the power intensity of the Raman laser (fig. 3 and figures S14 - 15). In order to probe the spin state change, we can follow the variation of the Raman modes below 400 cm^{-1} and in particular the Raman signals at 286 and 106 cm^{-1} corresponding to LS and HS states, respectively.²² The relative

LS fraction was estimated from the relative intensity of these two peaks $I_{289\text{cm}^{-1}}/(I_{289\text{cm}^{-1}}+I_{106\text{cm}^{-1}})$ and plotted as a function of the laser power in figure 3. It appears clearly that SCO particles associated with small gold nanoparticles (sample 2) need significantly less laser power to achieve the full LS to HS switch when compared to sample 1, which do not contain gold. Indeed, the power density applied to completely convert the iron sites from the LS to the HS state was ca. 9000 and 3000 W/cm^2 for 1 and 2, respectively. This finding was repeatedly obtained at different positions of the samples and using different laser wavelengths (633 nm and 532 nm). Thus, it is argued that due to their strong absorption at these wavelengths (see figure S18), the gold nanoparticles act as “nanoradiators” for the SCO material. Following the laser-induced LS to HS switch the sample remains in the HS state even if the laser is turned off. This observation (fig. S16) is quite expected since the temperature is fixed in the middle of the hysteresis loop. (*N.B.* Raman spectra before and after the laser-induced switch were recorded using a low excitation power (22 μW), which does not induce any spin state change in our experimental conditions.) In other words nanoparticles of both sample 1 and 2 function as a full optical, non-volatile switch. It is thus possible to store information in these particles and the grafting of gold particles allows to decrease the energy consumption for the writing process. A conceptually similar approach has been recently reported for a SCO material diluted in a polymer matrix.²³ In this case, the infrared laser induces a heating process of the host-matrix, which results in a localized modification of the properties of the sample.

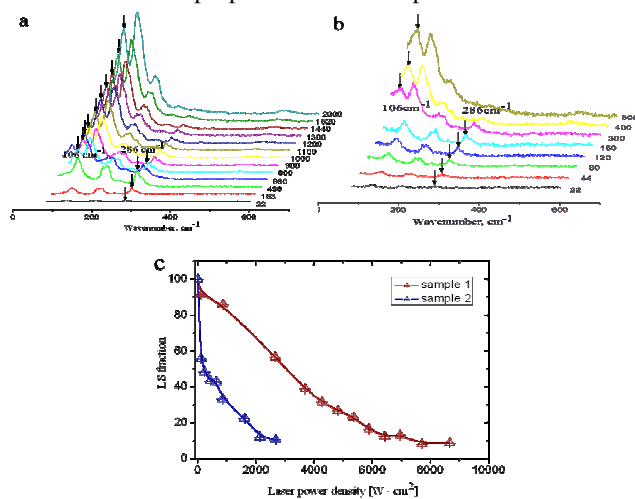


Figure 3. Raman spectra (excited at 633 nm) of 1 (a) and 2 (b) for increasing laser power densities and the corresponding laser power dependence of the LS fraction (c). (Lines are inserted to guide the eye.) During these experiments the sample stage was kept at 373 K.

Figure S17 shows the Raman spectrum obtained at room temperature for sample 3 (SCO@silica/larger gold Nps). All the attempts to get the Raman spectrum of the SCO complex were unsuccessful. This could be explained by the Surface Enhanced Raman Spectroscopy (SERS) effect.¹¹ SERS occurs when molecules are in contact with the surface of noble metals in a variety of morphologies. Thus, we have good reason to think that the SERS effect associated to this grafted larger gold nanoparticles with concomitant increase of surface contact becomes dominant and as a consequence it is difficult to get the characteristic Raman spectrum of the Fe(II) coordination polymer. This effect is supported by the thin silica shell but

nevertheless the distance between the gold nanoparticles and the complex is certainly too high to observe the enhancement of the vibrational modes of the iron complex. The observed spectrum is difficult to assign, since the Raman selection rules are also modified by the SERS effect, but certain modes may simply arise from the grafting ligand and/or the SiO_2 which are in close vicinity with the gold particles.

Conclusions

In this communication we described the synthesis of new SCO/gold nanocomposites, which were fully characterized for their composition, morphology and spin crossover properties. We have achieved a full low spin to high spin conversion in these samples using laser excitation and we have evidenced a plasmonic enhancement of this photo-thermal spin state switching effect. Despite the volume fraction of gold within the nanocomposite is only 0.5 % the laser power required for the complete spin transition is reduced by ca. 70 % even for low gold nanoparticles coverage. We expect that the threshold laser intensity can be still substantially reduced by increasing the amount of gold in the composites. Moreover, future works will focus on the variation of the spin crossover core and on the nature of the anchoring ligand and the metal nanoparticles.

Experimental Section

TEM images were obtained by using a JEOL JEM 1011 electron microscope operated at 100 kV. STEM and EDX measurements were carried out with a high-resolution microscope JEOL JSM 2100F operated at 200 kV. Samples for transmission electron microscopy were prepared by dispersing 5 mg of the material in 1 ml of ethanol and 2-3 drops of this suspension were deposited on a carbon covered copper grid. Grids then were dried in vacuum for at least 24 h. Raman spectra were recorded using a Labram-HR (Horiba Jobin Yvon) Raman spectrometer equipped with a Peltier-cooled CCD detector (Andor DU420) and an Olympus BXFMM optical microscope. 633 and 532 nm laser excitations were used. The laser beam was focused on a ca. 1.5 μm spot using a $\times 50$ magnification objective. The same objective was used to collect the scattered photons, which were filtered by an edge filter and dispersed by a 600 cm^{-1} grating to achieve a ca. 3 cm^{-1} spectral resolution. The laser intensity was adjusted using neutral density films and controlled by a PM100D Thorlabs power meter. Magnetic susceptibility data were collected with a Quantum Design MPMS-XL SQUID magnetometer at heating and cooling rates of 2 K/min^{-1} in the temperature range of 300 – 400 K and at a magnetic field of 1 kOe. ^{57}Fe Mössbauer spectra have been recorded using a conventional constant-acceleration type spectrometer equipped with a 50 mCi ^{57}Co source and a flow-type, liquid nitrogen cryostat. Spectra of the powder sample (ca. 50 mg) were recorded at 80 K. Least square fittings of the Mössbauer spectra have been carried out with the assumption of Lorentzian line shapes using the Recoil software package.

Notes and references

^aLaboratoire de la Chimie de Coordination, CNRS & Université de Toulouse (INPT, UPS), Toulouse, France

^bDepartment of Chemistry, National Taras Shevchenko University, 62 Vladimirska street, 01601 Kiev, Ukraine

† Electronic Supplementary Information (ESI) available: Synthesis details, electron microscopy images, magnetic, optical and spectroscopic data. See DOI: 10.1039/c000000x/

Acknowledgements

This work was financially supported by the project ANR-13-BS07-0020-01. IS thanks the French Embassy in Ukraine for financial support. JSC thanks the Marie-Curie research program (NanoSCOPE 328078). This work was performed in the frame of the International Associated Laboratory (LIA), Kiev–Toulouse.

- 1 Hybrid Materials. *Synthesis, Characterization, and Applications*. Edited by Guido Kickelbick, 2007 Wiley-VCH Verlag GmbH & Co. KGaA, Weinheim. ISBN: 978-3-527-31299-3.
- 2 F. Hoffmann, M. Cornelius, J. Morell, M. Froba, *Angew. Chem. Int. Ed.* 2006, **45**, 3216–3251.
- 3 O. Kahn, C. J. Martinez, *Science* 1998, **279**, 44 – 48.
- 4 A. Bousseksou, G. Molnar, L. Salmon, W. Nicolazzi, *Chem. Soc. Rev.* 2011, **40**, 3313-3335
- 5 P. Gütllich, A. Hauser and H. Spiering, *Angew. Chem., Int. Ed. Engl.*, 1994, **33**, 2024-2054.
- 6 T. Miyamachi, M. Gruber, V. Davesne, M. Bowen, S. Boukari, L. Joly, G. Rogez, P. Ohresser, E. Beaurepaire, W. Wulfhchel, *Nat. Commun.* 2012, **3**, 93
- 7 H. J. Shepherd, G. Molnar, W. Nicolazzi, L. Salmon and A. Bousseksou, *Eur. J. Inorg. Chem.*, 2013, 653-661.
- 8 G. Felix, K. Abdul-Kader, T. Mahfoud, I. A. Gural'skiy, W. Nicolazzi, L. Salmon, G. Molnár and A. Bousseksou, *J. Am. Chem. Soc.*, 2011, **133**, 15342-15345.
- 9 K. Abdul-Kader, M. Lopes, C. Bartual-Murgui, O. Kraieva, E. M. Hernandez, L. Salmon, W. Nicolazzi, F. Carcenac, C. Thibault, G. Molnár, A. Bousseksou, *Nanoscale*, 2013, **5**, 5288-5293.
- 10 G. Molnár, I.A. Gural'skiy, L. Salmon, W. Nicolazzi, C. Quintero, A. Akou, K. Abdel-kader, G. Félix, M. Lopes, Z. Pengxiang, D. Astruc, A. Bousseksou, *J. Nanophoton*, 2012, **6**, 063517.
- 11 C. Bartual-Murgui, A. Cerf, C. Thibault, C. Vieu, L. Salmon, G. Molnár, A. Bousseksou, *Microel. Eng.*, 2013, **11**, 365-368
- 12 Y. A. Tobon, C. Etrillard, O. Nguyen, J.-F. Letard, V. Faramarzi, J. F. Dayen, B. Doudin, D. M. Bassani, F. Guillaume, *Eur. J. Inorg. Chem.*, 2012, 5837-5842.
- 13 D. W. Ferrara, E. R. Macqarrie, J. Nag, A. B. Kaye, R. F. Haglund, *Appl. Phys. Lett.*, 2011, **98**, 241112.
- 14 E. Dreaden, A. Alkilany, X. Huang, C. Murphy and M. El-Sayed, *Chem. Soc. Rev.*, 2012, **41**, 2740–2779
- 15 O. Roubeau, *Chem. Eur. J.* 2012, **18**, 15230–15244
- 16 P. Durand, S. Pillet, E. Bendeif, C. Carteret, M. Bouazaoui, H. El Hamzaoui, B. Capoen, L. Salmon, S. Hebert, J. Ghanbaja, L. Arandah and D. Schanielab, *J. Mater. Chem. C*, 2013, **1**, 1933–1942.
- 17 C. Faulmann, J. Chahine, I. Malfant, D. Caro, B. Cormary and L. Valade, *Dalton Trans.*, 2011, **40**, 2480-2485.
- 18 S. Titos-Padilla, J. M. Herrera, X.-W. Chen, J.J. Delgado, E. Colacio, *Angew. Chem. Int. Ed.* 2011, **50**, 3290-3293.
- 19 C. Graf, A. Blaaderen, *Langmuir*, 2002, **18**, 524-534.
- 20 D. G. Duff, A. Baiker, I. Gameson, P. Edwards, *Langmuir* 1993, **9**, 2310-2317
- 21 J. Kröber, J.-P. Audière, R. Claude, E. Codjovi, O. Kahn, J. G. Haasnoot, F. Grolière, C. Jay, A. Bousseksou, J. Linares, F. Varret, A. Gonthier-Vassal, *Chem. Maert.*, 1994, **6**, 1404-1412.
- 22 N.O. Moussa, D. Ostrovskii, V.M. Garcia, G. Molnár, K. Tanaka, A.B. Gaspar, J.A. Real, A. Bousseksou, *Chem. Phys. Lett.* 2009, **477**, 156.
- 23 W. Hellel, A. O. Hamouda, J. Degert, J. F. Létard, E. Freysz, *Appl. Phys. Lett.* 2013, **103**, 143304.